Applied Catalysis A: General 435–436 (2012) 187–196

Contents lists available at SciVerse ScienceDirect

Applied Catalysis A: General

journal homepage: www.elsevier.com/locate/apcata

Influence of the Brönsted and Lewis acid sites on the catalytic activity and selectivity of Fe/MCM-41 system

N.A. Fellenz[a], J.F. Bengoa[b,1], S.G. Marchetti[b,*], A. Gervasini[c,**]

[a] Universidad Nacional de Rio Negro, Sede Atlántica, Belgrano 526, 8500, Viedma, Rio Negro, Argentina
[b] CINDECA, CONICET, CICPBA, UNLP, Fac. Ciencias Exactas, Calle 47, N◦. 257, 1900, La Plata, Argentina
[c] Dipartimento di Chimica Fisica ed Elettrochimica (DCFE) and Centro Interdipartimentale Materiali e Interfacce Nanostrutturati (CIMaINa), Università degli Studi di Milano, via Camillo Golgi, 19, 20133 Milano, Italy

ARTICLE INFO

Article history:
Received 26 March 2012
Accepted 2 June 2012
Available online 9 June 2012

Keywords:
POX isomerization
Lewis acid sites
MCM-41
Mössbauer spectroscopy

ABSTRACT

The system Fe_2O_3/MCM-41, with high iron dispersion, was synthesized in order to introduce Lewis acid sites into the MCM-41 structure. Two calcination atmospheres (inert and oxidant) were used to produce iron nanoclusters with different structural properties. Besides, a silylation treatment was realized on both solids with the aim of neutralizing the Brönsted acidity associated with the MCM-41 silanol groups. The samples were characterized by atomic absorption spectroscopy, X-ray diffraction at low angles, N_2 adsorption, temperature-programmed reduction, Fourier transform infrared spectroscopy, nuclear magnetic resonance of ^{29}Si, and Mössbauer spectroscopy. The influence of the structural changes of the nanoclusters and the effect of the simultaneous presence of Lewis and Brönsted acid sites were evaluated studying the product distribution from the α-pinene oxide isomerization reaction. It was determined that the Brönsted acidity of the Fe/MCM-41 system has not the sufficient acid strength to modify the product distribution which is mainly governed by the Lewis sites.

1. Introduction

In order to replace the conventional homogeneous acid catalysts (such as metal halides, HF and H_2SO_4) in many fine chemical reactions, numerous researches with solid acids had been made in the last decades. Solid acid catalysts with protonic acidity (Brönsted acid sites) have been better developed than Lewis acid containing catalysts [1–3], in particular zeolite materials. Many oxides containing dispersed metal centers on different supports appear good candidates as Lewis acid catalysts and they have been displayed interesting catalytic performances in reactions where Lewis acid centers are concerned [4,5]. Among them, the Fe_2O_3/SiO_2 system, with the high degree of coordinative unsaturation of the nanosized Fe_2O_3 clusters gives excellent catalytic properties in acid reactions, such as Friedel–Crafts alkylations [6,7]. A method to obtain such samples with the required Lewis acid sites is supporting "nanoclusters" of iron oxides on silica materials. In order to avoid the diffusional hindrance of large reactive molecules, mesoporous silicas with tuneable pore size could be used as supports for highly dispersed iron species. In this perspective, the Fe/MCM-41 system was selected in order to produce active and selective catalysts with Lewis acid sites associated with the Fe presence. However, it must be considered that the bare surface of MCM-41 has a great number of silanol groups, which have Brönsted acidity that adds up to the introduced Lewis acid sites of the Fe species [8].

To investigate on the acid properties and catalytic performances of the Fe/MCM-41 system, the α-pinene oxide (POX) isomerization reaction was taken into account; information on the Brönsted or Lewis catalytic action can be inferred from the obtained product distribution [9]. Moreover, the POX isomerization is an interesting reaction of fine chemistry, because one of the main products, campholenic aldehyde (CPA), is a very important intermediate used for the manufacture of sandalwood fragrances, currently being investigated together with macrocyclic musks, as possible substitutes for nitro and polycyclic musks, which are widespread used as fragrances in laundry detergents, fabric softeners, cleaning agents and cosmetic products, and are recognized as damaging chemical species to the environment.

Taking into account the co-presence of both the two kinds of acid sites (Brönsted and Lewis type) on the Fe/MCM-41 system, one aim of this work is to study the product distribution from the POX isomerization obtained on different Fe/MCM-41 samples with presence or suppression of the Brönsted acid sites of MCM-41, by evaluating the acid-strength of the different site-types, too. In order

---

* Corresponding author. Tel.: +54 221 4210711; fax: +54 221 4211353.
** Corresponding author. Tel.: +39 02 50314254; fax: +39 02 50314300.
E-mail addresses: nfellenz@quimica.unlp.edu.ar (N.A. Fellenz), bengoajf@quimica.unlp.edu.ar (J.F. Bengoa), march@quimica.unlp.edu.ar (S.G. Marchetti), antonella.gervasini@unimi.it (A. Gervasini).
[1] Tel.: +54 221 4210711; fax +54 221 4211353.

0926-860X/$ – see front matter © 2012 Elsevier B.V. All rights reserved.
http://dx.doi.org/10.1016/j.apcata.2012.06.003

to get this purpose, the surface silanol groups were replaced by trimethylsilyl groups using a silylation treatment. On the other hand, the possibility of generate different iron Lewis acid sites in the Fe/MCM-41 system, changing the calcination atmospheres (inert and oxidant), was studied too. The consequences produced by these treatments on the sample properties were studied by different characterization techniques and evaluated analyzing their influence on the selectivity and the activity on POX reaction.

2. Experimental

2.1. Catalyst preparation

MCM-41 support was prepared according to the methodology proposed by Ryoo and Kim [10] using sodium silicate as silica source, cetyl-trimethyl-ammonium chloride as surfactant under controlled pH during the hydrothermal synthesis. For the preparation of 16 g of sample, 40 g of sodium silicate (26.1% SiO_2) was dissolved into 74 g of water. The solution was then slowly added to 38 ml of cetyl-trimethyl-ammonium chloride and 0.65 ml of NH_3 under vigorous stirring at room temperature. This mixture was heated at 373 K for 24 h in a polypropylene bottle without stirring. Afterwards, it was cooled at room temperature. Then, the pH value was regulated to approximately 11 by drop wise addition of acetic acid under vigorous stirring. The reaction mixture was heated again at 373 K for 24 h. This procedure for pH control and subsequent heating was repeated twice. The resulting solid was filtered, washed and dried in air at room temperature. The surfactant was removed by calcination in N_2 flow (150 cm^3/min) heating the solid from room temperature to 783 K (8 K/min) maintaining the final temperature for 1 h. Finally, the N_2 flow was replaced by air, and the solid remained at 783 K for 6 h under air flowing.

The synthesized MCM-41 was impregnated by the incipient wetness impregnation method with $Fe(NO_3)_3 \cdot 9H_2O$ aqueous solution to produce a nominal Fe loading of 8% (w/w) in a single step. The solid was dried in air at room temperature, and then was split in two fractions; the first fraction was calcined in a flow of N_2 (60 cm^3/min) from room temperature to 603 K (0.2 K/min), and kept at the final temperature for 1 h, so obtaining the Fe/MCM-41(N2) sample. The second fraction was calcined under the same conditions above described, replacing the nitrogen flow by air, so obtaining the Fe/MCM-41(air) sample.

A fraction of both solids was silylated with hexamethyldisilazane (HMDS). In order to get this treatment the solids were outgassed ($p_v < 10^{-3}$ Torr) during 3 h at 573 K. Then, a solution of 1% (v/v) of HMDS in toluene was prepared in a glove box, in Ar atmosphere, and it was added to the dehydrated solids. The mixture was heated at 393 K, during 90 min under stirring. Finally, the treated solids were filtered, washed with 80 cm^3 of toluene, and dried in an oven at 333 K during 16 h. The obtained solids were called Fe/MCM-41(N2)-sil and Fe/MCM-41(air)-sil taking into account the nature of the calcination atmospheres.

2.2. Catalyst characterization

The samples were characterized by atomic absorption spectroscopy (AAS), X-ray diffraction (XRD) at low angles, N_2 adsorption at 77 K (BET), temperature-programmed reduction (TPR), Fourier transform infrared spectroscopy (FT-IR), nuclear magnetic resonance (NMR) of ^{29}Si, and Mössbauer spectroscopy (MS) at 298 and 25 K.

The Fe content of the solids was determined by atomic absorption on an AA/AE Spectrophotometer 457 of Laboratory Instrumentation Inc. The sample was treated in a mixture of HCl and HF up to complete dissolution before measurement.

All XRD patterns at low angles were measured using a standard automated powder X-ray diffraction system Philips PW 1710 with diffracted-beam graphite monochromator using Cu Kα radiation ($\lambda = 1.5406$ Å) in the range $2\theta = 0.5–9^\circ$ with steps of 0.02° and counting time of 2 s/step.

The textural properties, specific surface area (S_g), specific pore volume (V_p) and pore diameter (D_p), were measured in Micromeritics equipment ASAP 2020 V1.02 E.

The TPR profiles were obtained in a Quantachrome equipment, model Quantasorb Jr. The samples (≈50 mg) were reduced between 300 and 1273 K, at a heating rate of 10 K/min, using a 5% H_2/N_2 mixture. Taking into account the reducible amount of iron oxide in the samples, "K" (the sensitivity parameter expressed in s) and "P" (the shape and resolution parameter, expressed in K) [11] were around 75 s and 15 K, respectively.

The FT-IR absorption spectra were acquired with a Bruker IFS66 spectrometer with 1 cm^{-1} resolution by co-addition of 32 scans. The samples were prepared mixing with potassium bromide, in a 1:100 proportion, in order to obtain the corresponding pellets.

Solid state ^{29}Si nuclear magnetic resonance spectra by direct polarization (DP) and cross-polarization (CP) ^1H—^{29}Si with proton decoupling and magic angle spinning (MAS) were recorded on a Bruker Avance II-300 spectrometer equipped with a 4-mm MAS probe operating at 300.13 MHz for protons and 59.6 MHz for ^{29}Si. Magic angle spinning rate was 5 kHz. Other experimental conditions were: cw proton decoupling at 62.5 kHz, contact time for CP 5 ms. The chemical shifts are given in ppm from H_3PO_4 (0 ppm) as standard reference.

The Mössbauer spectra were obtained in transmission geometry with a 512-channel constant acceleration spectrometer. A source of ^{57}Co in Rh matrix of nominally 50 mCi was used. Velocity calibration was performed against a 12 μm-thick α-Fe foil. All isomer shifts (δ) mentioned in this paper are referred to this standard. The temperature was varied between 25 and 298 K using a Displex DE-202 Closed Cycle Cryogenic System. The Mössbauer spectra were evaluated using a commercial program with constraints named Recoil [12]. Although some spectra display magnetic relaxation, for simplicity, Lorentzian lines with equal widths were considered for each spectrum component. The spectra were folded to minimize geometric effects.

2.3. Activity and selectivity measurements

The epoxide isomerization tests using POX as substrate were carried out at room temperature (RT) in batch conditions as detailed in Refs. [9,13]. The catalyst sample (0.1 g) was activated into the glass reactor at 623 K for 30 min in air and then for 30 min under reduced pressure at the same temperature. After catalyst activation, α-pinene oxide (0.66 mmol) and toluene (8 ml) were introduced into the reactor under N_2 atmosphere. The progress of the reaction was followed by gas-chromatographic techniques (GC from Agilent 6890 with FID detector, with a 5% phenyl-methylpolysiloxane column, and GC–MS from Agilent 5971 series), analyzing samples withdrawn from the reaction mixture at different times.

3. Results and discussion

3.1. Catalyst characterization and silylation effect

The ordered hexagonal structure of mesoporous MCM-41, used as support, was verified by XRD (Fig. 1) and its textural properties were measured by N_2 adsorption at 77 K (Table 1). The impregnation, calcination in different atmospheres, and silylation treatments, which lead to Fe/MCM-41(N2), Fe/MCM-41(N2)-sil,

Table 1
Textural properties and iron loading of the studied catalyst samples.

Samples	S_g (m^2/g)	D_p(nm)	V_p (cm^3/g)	C_{BET}	%Fe (w/w)
MCM-41	912	2.7	0.88	107	–
Fe/MCM-41(N2)	691	2.9	0.64	108	8.9
Fe/MCM-41(N2)-sil	494	2.4	0.59	45	8.6
Fe/MCM-41(air)	608	2.6	0.50	92	8.4
Fe/MCM-41(air)-sil	476	2.6	0.33	62	8.4

S_g, specific surface area; D_p, average pore diameter; V_p, specific pore volume; C_{BET}, BET model constant.

Fe/MCM-41(air), and Fe/MCM-41(air)-sil, did not change the structural properties of the mesoporous support, as was verified by XRD (Fig. 1).

By analyzing the textural properties of Fe/MCM-41(N2), and Fe/MCM-41(air), a decrease of S_g and V_p in comparison with the support, without substantial changes in D_p, can be observed (Table 1). This would imply a partial pore filling of the support with the Fe oxide species. After the silylation treatment these results were more pronounced and they were attributed to the covering of the internal pore walls with trimethylsilyl groups. Similar results were reported by other authors [14,15].

The Fe loading, obtained by AAS, can be considered similar over all the catalysts within acceptable experimental errors (Table 1), so strengthening the possibility of comparison among all samples.

The MCM-41 mesoporous solid has a great number of silanol groups (Si—OH) with pronounced hydrophilic character which are distributed on the inner surface of the channels. The deposition of Fe on MCM-41 should change the nature of the acid surface turning towards surfaces with prevalent Lewis acidity [9,13,16]. However, Brönsted acidity remains on the Fe-samples due to some silanol group presence. A silylation treatment was realized to decrease the number of Brönsted acid sites, and so changing the Lewis/Brönsted acid sites ratio. Besides, this treatment would modify the hydrophilic/hydrophobic nature of these catalysts. In order to study the influence of both effects on the catalytic performance, a reaction test, in which acidic sites are concerned, was selected: isomerization of α-pinene oxide. This reaction allows studying the prevalent presence of Lewis or Brönsted acid sites, through the influence of the acid-site nature on the activity and particularly on selectivity of the formed products.

In order to get the surface hydrophobization and nullify the silanol group action, Fe/MCM-41(N2) and Fe/MCM-41(air) were contacted with HMDS to produce trimethylsilyl groups according to the following scheme [17]:

$$2{\equiv}\mathrm{Si{-}OH} + (\mathrm{CH_3})_3\mathrm{{-}Si{-}NH{-}Si{-}}(\mathrm{CH_3})_3$$
$$\rightarrow\ 2{\equiv}\mathrm{Si{-}O{-}Si{-}}(\mathrm{CH_3})_3 + \mathrm{NH_3}$$

In order to verify the silylation treatment efficiency, the C_{BET} value obtained from N_2 adsorption measurements at 77 K, was analyzed. Taking into account that the magnitude of C_{BET} is an indication of the adsorption enthalpy between the adsorbate (N_2) and the solid surface, a smaller C_{BET} value would indicate a weaker interaction between N_2 molecules and the solid surface [18]. By comparing Fe/MCM-41(N2) and Fe/MCM-41(N2)-sil catalysts, a decreasing of 2.4 times of the C_{BET} value can be observed as a consequence of the silylation treatment (Table 1) which is indicative of the presence of a hydrophobic surface. In the same way, Fe/MCM-41(air)-sil showed a decreasing of 1.5 times of its C_{BET} value with respect to Fe/MCM-41(air).

The H^+ substitution of the silanol groups by trimethylsilyl groups can be monitored by FT-IR [15,19]. With this purpose, the IR spectra of Fe/MCM-41(N2) and Fe/MCM-41(N2)-sil were collected (Fig. 2). In Fe/MCM-41(N2)-sil spectrum, two new bands can be distinguished: the 758 cm^{-1} band is assignable to the stretching of Si—C bond and the 849 cm^{-1} band to rocking of CH_3 groups [15]. According to Lin et al. [19] these results indicate that trimethylsilyl groups of the silylant agent were anchored on the mesoporous solid surface. Therefore, these results point to the same direction that the analysis on the C_{BET} value, indicating that the surface silylation process, used in this work, was successful. Similar results were obtained with Fe/MCM-41(air) and Fe/MCM-41(air)-sil (not shown).

More information about the efficiency of the silylation treatment was obtained from the ^{29}Si NMR spectra. The measurement of the NMR spectra of Fe/MCM-41(N2), Fe/MCM-41(N2)-sil, Fe/MCM-41(air) and Fe/MCM-41(air)-sil was prevented due to the magnetic behavior of the samples; they were all weak-ferromagnetic. Therefore, the ^{29}Si NMR spectra were obtained with a sample of MCM-41 without Fe, before and after silylation treatment (MCM-41 and MCM-41-sil). The presence of Fe^{3+} centers, acting as Lewis acid sites, may become more acidic the neighbor silanol groups [13]. Therefore we consider that, if the silylation treatment is effective without iron, a greater efficiency would occur when it is present. The NMR spectra of MCM-41 and MCM-41-sil obtained by DP are shown in Fig. 3. For both samples, the most intense peak appears at −110 ppm, and it is associated with silicon atoms bonded to four siloxane groups, such as $(SiO_4)Si$. A shoulder at about −101 ppm can be also observed, which is assigned to the presence of silanol groups bonded to a surface silicon atom $(SiO_3)Si{-}OH$ [17]. Besides, a peak at about 14 ppm is only observed for MCM-41-sil. This signal can be assigned to $(CH_3)_3{-}Si{-}$ species [15,20]. In Fig. 4 the NMR spectra by CP $^1H{-}^{29}Si$ with proton decoupling and MAS are reported. In these experiments, the signals of ^{29}Si atoms surrounded by protons are reinforced with respect to other Si atoms. This effect can be clearly observed when Figs. 3 and 4 are compared. Therefore, the assignments for the peaks at −101 and 14 ppm, made by DP, are right, confirming that MCM-41-sil was silylated.

Therefore, N_2 adsorption results, FT-IR and NMR spectra allow us to conclude that the silylation treatment was successfully and hydrophobic surfaces were attained. However, it is important to remark that this process is not totally effective since some silanols groups remain on the surface as it is evidenced in ^{29}Si RMN spectrum by the shoulder at −101 ppm.

In order to characterize the iron species present at the catalysts, Mössbauer spectra at different temperatures were collected. The Mössbauer spectrum of Fe/MCM-41(N2) at 298 K shows a very intense central doublet and a small sextuplet (Fig. 5). The hyperfine parameters of the sextuplet correspond to α-Fe_2O_3 [21] (Table 2). The hyperfine magnetic field (H) is lower than that corresponding to the “bulk”, probably due to the small size of the α-Fe_2O_3 crystals. This decrease in the H value could be attributed to the magnetic collective excitations phenomenon [22]. Applying this model and using an effective magnetic anisotropy constant $K_{CME} = 3.5 \times 10^3$ J/m^3 [23], a rough estimation of the average diameter value of crystal oxide of about 35 nm for the magnetic fraction was obtained. Taking into account that the average pore diameter of the support is about 3 nm (Table 1) is evident that this fraction of

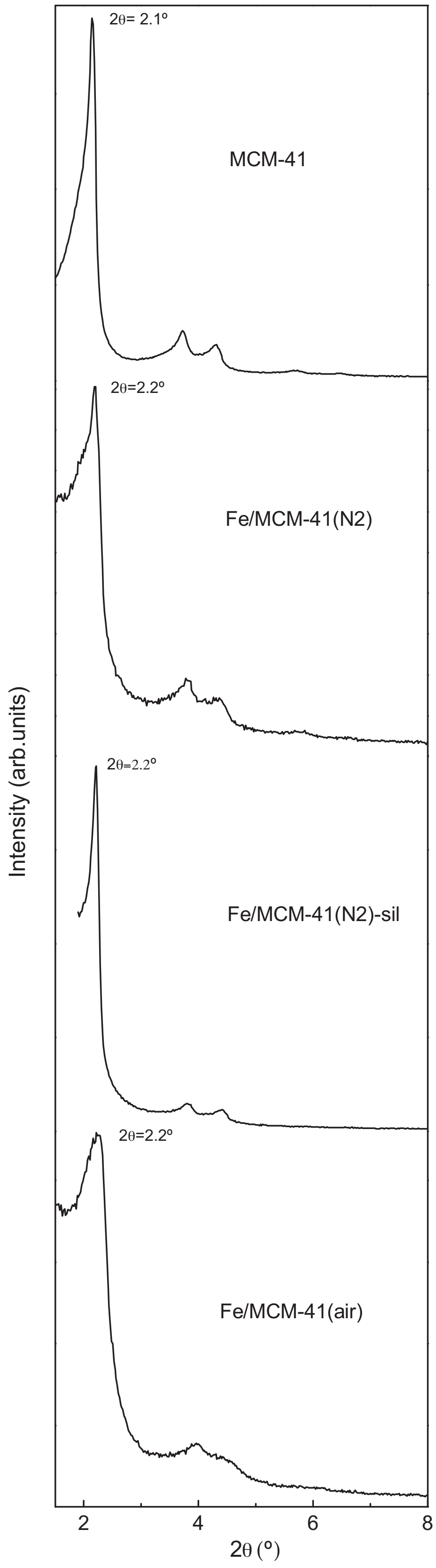

Fig. 1. XRD patterns at low angles of the support and the catalysts.

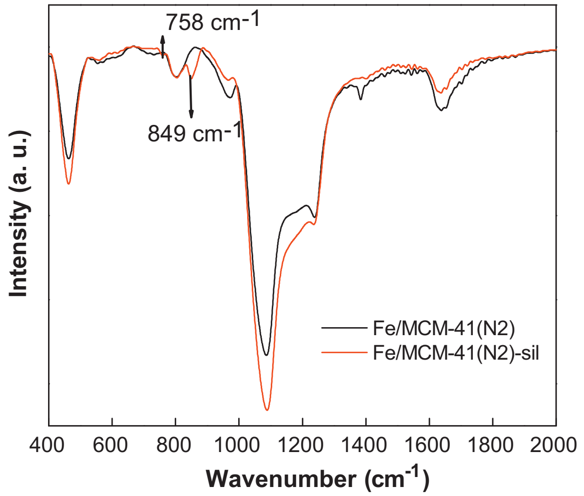

Fig. 2. FT-IR spectra of Fe/MCM-41(N2) before and after silylation treatment.

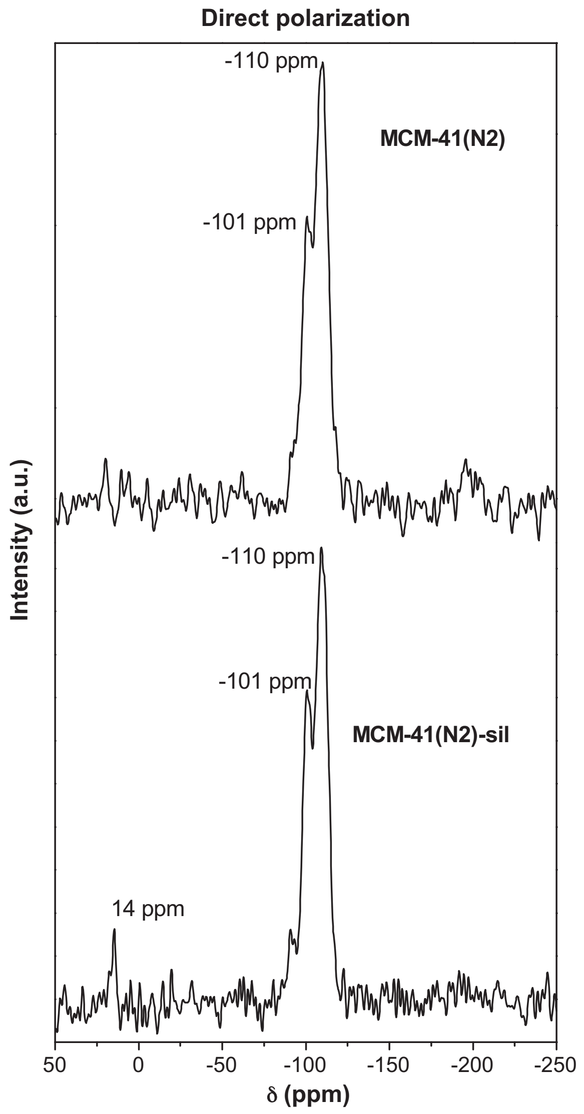

Fig. 3. NMR spectra of MCM-41 and MCM-41-sil obtained by direct polarization.

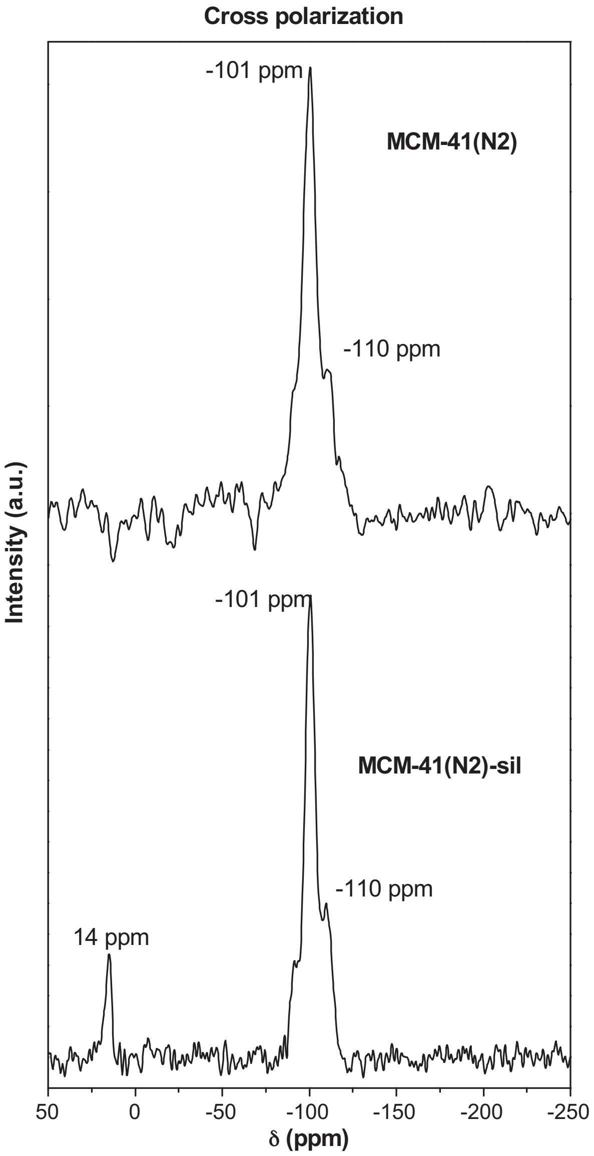

Fig. 4. NMR spectra of MCM-41 and MCM-41-sil obtained by cross polarization.

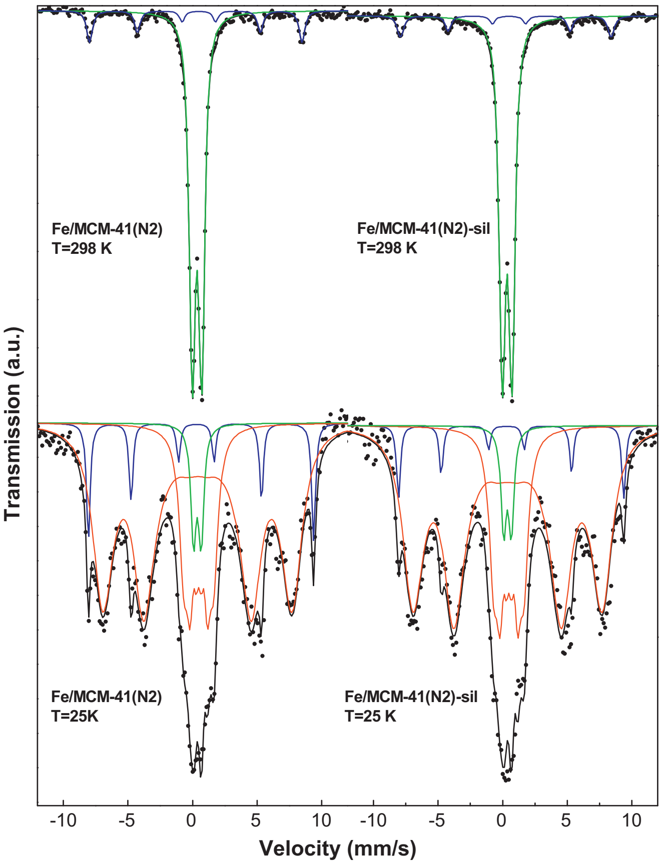

Fig. 5. Mössbauer spectra of Fe/MCM-41(N2) and Fe/MCM-41(N2)-sil at 298 and 25 K.

the iron species is located outside the channels of the MCM-41. The doublet could be assigned to superparamagnetic α-Fe_2O_3 particles (α-Fe_2O_3 (sp)), smaller than those that produce the sextuplet, or to paramagnetic Fe^{3+} ions diffused into the support walls.

To select the right option, the Mössbauer spectrum at 25 K was obtained (Fig. 5). The spectrum displayed a broad central line and three peaks at both sides, two of them are broad and the other narrow. Comparing this spectrum with that obtained at 298 K is obvious that the superparamagnetic relaxation phenomenon is present; the background is curved, there are very broad peaks and the central signal had decreased but it had not disappeared. Therefore, this complex behavior was fitted with three sextets and one doublet. Two sextuplets are relaxing and they were simulated using the relaxation model of two states of Blume and Tjon [24] and the other one (the narrower) is non-relaxing. This non-relaxing sextet has parameters of α-Fe_2O_3 which has undergone Morin transition, therefore, their diameters are larger than ≈20 nm [25] (called α-Fe_2O_3 in Table 2). The second sextet has not completed the magnetic blocked state, yet (called partially magnetically blocked α-Fe_2O_3 in Table 2). The third sextet is in relaxation process with a fluctuation speed higher than the previous one (called relaxing α-Fe_2O_3 in Table 2). The evolution of these two broad sextets when the temperature decreased would indicate that at lower temperature the magnetic blocking process would be completed; and the hyperfine parameters would corresponds to α-Fe_2O_3 with extremely small sizes. Anyway, the presence of amorphous Fe_2O_3 “nanoclusters” cannot be excluded since the hyperfine magnetic fields are much decreased. This complex magnetic behavior prevents to determine the right value of the blocking temperature (T_B) of the sample (defined as the temperature at which 50% of the sextet components have collapsed to doublets). However, a value of about 25 K for T_B can be estimated.

By applying the Neel–Brown relaxation model [26] and using a basal magnetic anisotropy constant $K_{BU} = 2.4 \times 10^4\ J/m^3$, determined by Bødker and Mørup [23] for hematite particles of 5.9 nm size, a rough estimation of the average diameter value of crystal oxide of about 3 nm for the fraction of α-Fe_2O_3 (sp) at 298 K, was obtained. By considering this result jointly with the textural measurements, we can conclude that the iron species are predominantly located inside the MCM-41 channels. Finally, the small doublet (5 ± 2%) that remains at this low temperature can be assigned to paramagnetic Fe^{3+} ions diffused into the MCM-41 walls. Therefore, in Fe/MCM-41(N2) there should be two fractions of α-Fe_2O_3 with very different sizes: a small percentage, 8 ± 1% of crystals of about 35 nm located outside of the MCM-41 channels structure and the great majority as extremely small crystals that even at 25 K do not get blocked magnetically, located inside the MCM-41 channels.

In order to verify that the silylation treatment did no affect the nature and the size of the iron species present in the catalyst, the Mössbauer spectra of Fe/MCM-41(N2)-sil at 298 and 25 K were obtained (Fig. 5). It can be seen that the fitting and the hyperfine

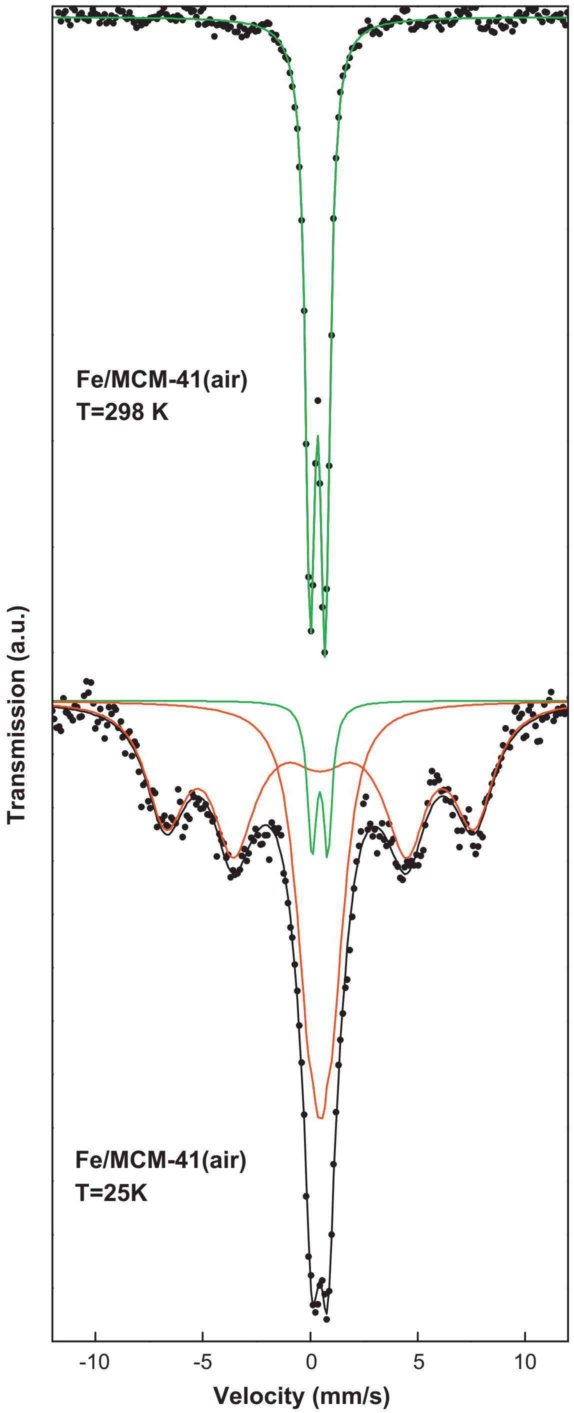

Fig. 6. Mössbauer spectra of Fe/MCM-41(air) at 298 and 25 K.

parameters obtained at both temperatures (Fig. 5 and Table 2) are identical – within the experimental errors – to that obtained before the silylation treatment.

The Mössbauer spectra of Fe/MCM-41(air) at 298 and 25 K are shown in Fig. 6. At 298 K only a doublet had been detected assignable to α-Fe_2O_3 (sp) or to paramagnetic Fe^{3+} ions diffused into the support walls. It is important to remark that the magnetic signal, corresponding to α-Fe_2O_3 located outside the MCM-41 channels, was not detected. Again, the spectrum obtained at 25 K showed a superparamagnetic relaxation with a partial magnetic blocking. Two relaxing sextuplets and a doublet were used in the fitting process. Both sextets were assigned, in the same way that in Fe/MCM-41(N2), to α-Fe_2O_3 with different magnetic relaxation speeds. For the same reasons that in this solid the presence of amorphous Fe_2O_3 "nanoclusters" cannot be discarded. Taking into account that at 25 K, the magnetic blocking is lower than in Fe/MCM-41(N2), we can conclude that the iron oxide particles are lower than 3 nm. The doublet was assigned to paramagnetic Fe^{3+} ions diffused into the MCM-41 walls. Its percentage was nearly equal to that obtained with Fe/MCM-41(N2): 5 ± 2% for Fe/MCM-41(N2) vs. 7 ± 3% for Fe/MCM-41(air). Therefore, in Fe/MCM-41(air) were detected the same species that in Fe/MCM-41(N2), but all iron oxide crystals are located inside of the MCM-41 pores and its average diameter is smaller. Taking into account that the impregnation step was common in both systems, we can conclude that during the calcination step in N_2 stream, a fraction of the iron crystals migrate outside of the MCM-41 pores and growth up by sintering process. In a previous work [27] a similar result was obtained by studying the effect of the calcination atmospheres on the structural properties of Fe/amorphous SiO_2 system. These results were explained taking into account that the solid–solid wetting phenomenon can be drastically modified when the composition of the gaseous environment is changed. Thus, it has been established that the condition by spreading of the iron oxide on the support is more easily satisfied in oxidant atmosphere [28]. Therefore, in Fe/MCM-41(air) the spreading conditions could be satisfied more easily, leading to the production of islands like as "raft" of iron oxide. These "rafts" would strongly interact with the inner walls of the MCM-41 channels, and their migration at the outside surface would be hindered.

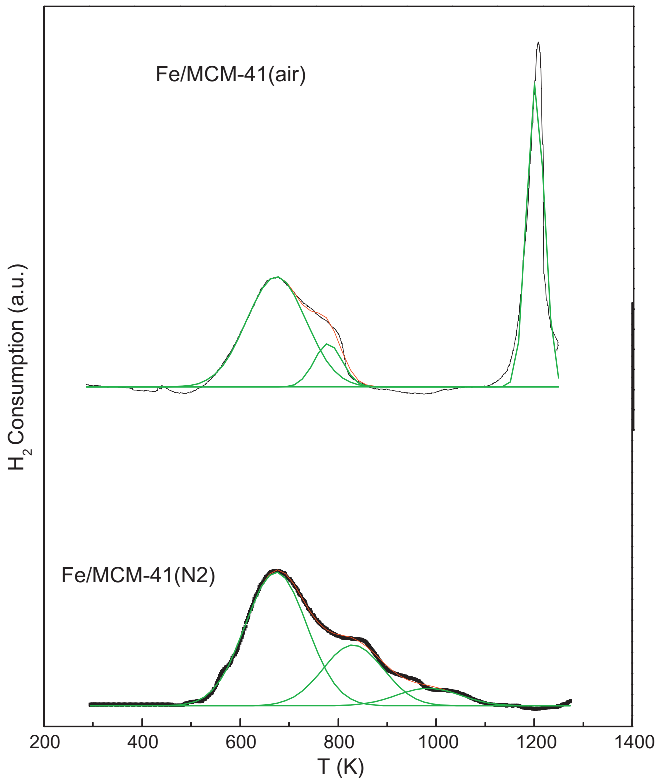

Fig. 7. TPR profiles of Fe/MCM-41(N2) and Fe/MCM-41(air).

In order to confirm these different interaction strengths between the iron oxides species and the MCM-41 support – depending on the used calcination atmosphere- the TPR assays with Fe/MCM-41(N2) and Fe/MCM-41(air) were obtained (Fig. 7). The Fe/MCM-41(N2) TPR profile was fitted with three Gaussian peaks

Table 2
Mössbauer parameters of the catalyst samples measured at 298 K and 25 K.

Temperature	Species	Parameters	Fe/MCM-41 (N2)	Fe/MCM-41 (N2)-syl	Fe/MCM-41 (air)
298 K	α-Fe_2O_3	H (T)	51.0 ± 0.2	50.5 ± 0.2	–
		δ (mm/s)	0.37 ± 0.03	0.37 ± 0.03	–
		2ε (mm/s)	−0.24 ± 0.06	−0.26 ± 0.06	–
		%	15 ± 1	11 ± 1	–
	α-Fe_2O_3 (sp) and/or paramagnetic Fe^{3+}	Δ (mm/s)	0.73 ± 0.01	0.75 ± 0.01	0.70 ± 0.01
		δ (mm/s)	0.35 ± 0.01	0.35 ± 0.01	0.35 ± 0.01
		%	85 ± 1	89 ± 1	100
25 K	α-Fe_2O_3	H (T)	54.1 ± 0.2	54.0 ± 0.2	–
		δ (mm/s)	0.47 ± 0.02	0.47 ± 0.04	–
		2ε (mm/s)	0.37 ± 0.05	0.33 ± 0.07	–
		%	8 ± 1	5 ± 1	–
	Partially magnetically blocked α-Fe_2O_3	H (T)	45.8 ± 0.4	46.1 ± 0.3	45.2 ± 0.8
		δ (mm/s)	0.38 ± 0.04	0.50 ± 0.03	0.45 ± 0.07
		2ε (mm/s)	0*	0*	0*
		%	66 ± 3	66 ± 3	57 ± 6
	Relaxing α-Fe_2O_3	H (T)	41.5*	41.5*	41.5*
		δ (mm/s)	0.48 ± 0.06	0.48 ± 0.04	0.47 ± 0.03
		2ε (mm/s)	0*	0*	0*
		%	21 ± 3	22 ± 2	37 ± 5
	Paramagnetic Fe^{3+} diffused into MCM-41 walls	Δ (mm/s)	0.59 ± 0.07	0.59 ± 0.06	0.7 ± 0.1
		δ (mm/s)	0.37 ± 0.04	0.37 ± 0.04	0.45 ± 0.04
		%	5 ± 2	7 ± 1	7 ± 3

H: hyperfine magnetic field in Tesla; δ: isomer shift (all the isomer shifts are referred to α-Fe at 298 K); 2ε: quadrupole shift; Δ: quadrupole splitting.

* Parameters held fixed in fitting.

with maxima at 673, 830 and 986 K. They could be assigned to the following reduction steps:

$$\alpha\text{-}Fe_2O_3/\text{amorphous}Fe_2O_3 \rightarrow Fe_3O_4 \rightarrow FeO \rightarrow \alpha\text{-}Fe$$

Beyond 1250 K, the profile showed a small increase that could be attributed to the beginning of the Fe^{2+} ions reduction diffused inside the SiO_2 walls. The Fe/MCM-41(air) TPR profile showed important differences with respect to Fe/MCM-41(N2). Thus, only the two first peaks were detected at 712 and 826 K. The third peak assigned to the reduction of FeO to α-Fe did not appear. Instead, a very intense H_2 consumption was detected at 1283 K. Taking into account the high temperature of this peak, it could be attributed to the reduction of Fe^{2+} ions diffused inside the MCM-41 walls. A great quantity of this species would be produced after the FeO formation due to a very important interaction with the support. Therefore, the Fe^{2+} diffusion into the SiO_2 lattice competes with the final reduction. As consequence the FeO → α-Fe step at about 900–1000 K did not occur. This different reduction behavior would confirm the distinct interaction degree between iron oxide species and the support, and would justify the different crystal sizes obtained when the calcination atmospheres were changed.

3.2. Catalytic test of α-pinene oxide isomerization

The isomerization of POX can be viewed as a test for understanding the action of the Brönsted or Lewis acid sites and their relative ratio, besides its recognized importance in specialty chemistry [29–32]. In this work, it has been used as model reaction able to enlighten the presence of active catalytic Lewis sites from the product distribution [9,13]. The acid POX rearrangement can give several products since this molecule has a high reactivity (Fig. 8) [29]. Thus over acid catalysts, CPA, transcarveol (TCV), trans-sobrerol (TSB), pinocamphone (PCP), and paracymene (CIM) can be observed as the principal reaction products. Among them, CPA is the most interesting product since is a very important intermediate used for the manufacture of fragrances. High CPA selectivities from acid POX isomerization can be obtained only if Lewis acid sites are working at the catalyst surface [9]. Acid surfaces with presence of Brönsted acid sites lead to some other products, like PCP, TCV, and dimerization products, decreasing the CPA selectivity. In the present catalysts, Brönsted acid sites could be generated from silanol groups, especially if they are located near to the Fe^{3+} centers [13]. Since the silylation treatment is expected to decrease the number of silanol groups, the silylated Fe/MCM-41 samples may turn the product distribution towards species formed by the Lewis acid site transformation of POX.

The results obtained in the α-pinene oxide transformation over the four Fe/MCM-41samples are presented in Tables 3 and 4. Figs. 9 and 10 display the most significant results in terms of POX conversion and CPA selectivity. Fe/MCM-41(N2) catalyst showed a fast POX conversion during the first 10 min and the reaction proceeded up to complete POX conversion in about 30 min. Selectivity to CPA started at ca. 70% and it little decreased down to 60% at total POX conversion. It is important to remark that the TCV production is nearly negligible; therefore, the silanol groups did not have Brönsted acidity strong enough to produce this by-product. The silylation treatment (Fe/MCM-41(N2)-sil sample) did not remarkably show different results in terms of product distribution. Total POX conversion was achieved at longer time (60 min of reaction) in comparison with Fe/MCM-41(N2). We can conclude that the more hydrophobic nature of the surface – after the silylation treatment – makes more difficult the arrival of the polar reactive molecules up to the Fe^{3+} sites.

The catalytic test results over Fe/MCM-41(air) and Fe/MCM-41(air)-sil were very different from the same materials calcined in inert atmosphere. They showed very lower activity in terms of POX conversion but higher selectivity to CPA (Table 4 and Figs. 8 and 9). Reaction times as long as 24 h were necessary to obtain a complete POX conversion. The low initial POX conversion (around 10%) was accompanied by a very high initial selectivity to CPA (more than 90%) on both Fe/MCM-41(air) and Fe/MCM-41(air)-sil. For longer times of reaction POX conversion increased and selectivity to CPA little decreased; it was around 70% after 250 min of reaction. A certain degree of deactivation of the most active Lewis sites could be inferred to explain the observed fall of selectivity. The effect of the silylation treatment on Fe/MCM-41(air) was very similar to

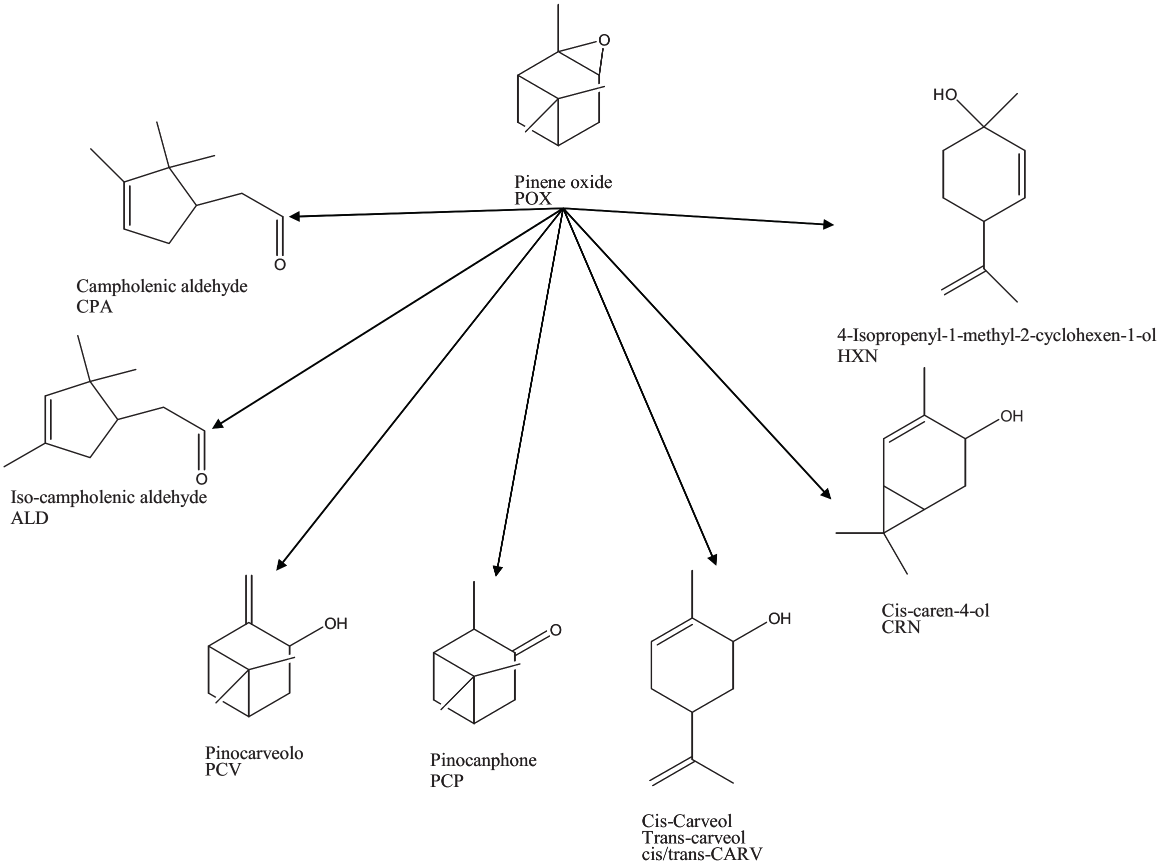

Fig. 8. Scheme of the α-pinene oxide isomerization reaction over Fe/MCM-41 catalysts.

that already observed over Fe/MCM-41(N2) and Fe/MCM-41(N2)-sil samples.

Taking into account the results obtained from the characterization study, we know that the iron species were the same in both sample series (calcined in inert and oxidant atmospheres), the most part of Fe-species are extremely small nanoparticles located inside the channels of the MCM-41 support (the population of large α-Fe_2O_3 particles in Fe/MCM-41(N2) is very small). Therefore, the observed different catalytic behavior would be assigned to more subtle structural differences. We can speculate that calcination in oxidant conditions helps the spreading of the iron species on the inner walls of the MCM-41 (more oxidant atmosphere) and favor the oxide/support interaction (as it was demonstrated by TPR); only one type of geometry of Fe^{3+} site is prevalently formed. These iron sites have high coordinative unsaturation and can act as acid Lewis sites in the catalytic reaction. All

Table 3
Catalytic performances of the Fe/MCM-41(N2) and Fe/MCM-41(N2)-sil catalysts in the reaction of isomerization of α-pinene oxide in terms of POX conversion and selectivity to all the products.

Catalyst code	Sample mass (g)	Reaction Time (min)	Conversion (%)	Selectivity (%)								
			POX	CPA	ALD	PCV	PCP	cis-CARV	trans-CARV	CRN	HXN	Other
Fe/MCM-41(N2)												
	0.1039	1	48.6	67.5	7.5	2.8	0.0	0.0	0.0	9.1	7.1	5.1
		3	64.1	66.2	7.4	2.9	0.0	0.0	0.0	8.9	7.4	6.4
		5	67.9	71.3	8.2	3.2	0.0	0.0	0.0	9.1	0.0	7.0
		10	85.0	60.8	7.3	2.8	1.3	2.0	2.0	9.1	7.7	6.2
		20	93.4	59.5	7.3	2.8	1.4	2.1	2.1	9.6	8.2	6.2
		30	97.6	59.3	7.3	2.8	1.4	2.0	2.2	9.7	8.3	6.2
Fe/MCM-41(N2)-sil												
	0.1042	1	30.5	75.9	0.0	3.9	0.0	0.0	0.0	7.5	5.2	7.0
		3	49.1	68.6	7.6	3.7	0.0	0.0	0.0	7.4	5.7	6.3
		5	59.6	66.6	7.9	3.6	0.0	0.0	0.0	8.3	6.3	6.4
		10	70.5	64.0	7.7	3.4	0.0	1.6	0.0	8.6	6.4	6.4
		20	76.8	66.9	8.2	3.4	0.0	0.0	0.0	8.0	6.1	6.4
		30	84.5	66.6	8.2	3.4	0.0	0.0	0.0	8.3	6.1	6.4
		60	95.5	59.9	7.8	3.1	1.3	2.0	2.1	9.2	7.0	6.3

POX: α-pinene oxide; CPA: campholenic aldehyde; ALD: iso-campholenic aldehyde; PCV: pinocarveol; PCP: pinocamphone; cis-CARV: cis-carveol; trans-CARV: trans-carveol; CRN: cis-caren-4-ol; HXN: 4-isopropenyl-1-methyl-2-cyclohexen-1-ol.

Table 4
Catalytic performances of the Fe/MCM-41(air) and Fe/MCM-41(air)-sil catalysts in the reaction of isomerization of α-pinene oxide in terms of POX conversion and selectivity to all the products.

Catalyst code	Sample mass (g)	Reaction Time (min)	Conversion (%)	Selectivity (%)								
			POX	CPA	ALD	PCV	PCP	cis-CARV	trans-CARV	CRN	HXN	Other
Fe/MCM-41(air)												
	0.1031	1	8.9	94.6	0.0	8.1	0.0	0.0	0.0	0.0	0.0	0.0
		3	11.0	91.9	0.0	9.5	0.0	0.0	0.0	0.0	0.0	0.0
		5	11.6	93.8	0.0	7.8	0.0	0.0	0.0	0.0	0.0	0.0
		10	15.2	90.4	0.0	9.1	0.0	0.0	0.0	0.0	0.0	0.0
		20	17.9	87.0	0.0	8.9	0.0	0.0	0.0	0.0	0.0	3.6
		30	24.1	76.9	9.2	8.6	0.0	0.0	0.0	0.0	0.0	4.4
		60	23.6	83.8	0.0	7.8	0.0	0.0	0.0	3.4	0.0	4.0
		120	31.2	76.0	8.0	7.0	0.0	0.0	0.0	4.2	0.0	3.8
		240	42.6	71.0	7.6	8.0	0.0	0.0	0.0	6.1	2.6	3.2
		1260	70.9	67.4	8.1	8.8	0.0	1.7	0.0	8.2	0.0	4.0
Fe/MCM-41(air)-sil												
	0.1022	1	8.0	93.6	0.0	8.6	0.0	0.0	0.0	0.0	0.0	0.0
		3	11.2	92.3	0.0	8.8	0.0	0.0	0.0	0.0	0.0	0.0
		5	14.7	88.8	0.0	9.5	0.0	0.0	0.0	0.0	0.0	0.0
		10	18.4	82.5	0.0	9.3	0.0	0.0	0.0	0.0	0.0	2.7
		20	19.2	89.3	0.0	8.8	0.0	0.0	0.0	0.0	0.0	0.0
		30	23.5	85.5	0.0	9.7	0.0	0.0	0.0	0.0	0.0	2.8
		60	30.2	78.1	0.0	8.4	0.0	0.0	0.0	6.0	2.4	2.9
		120	44.8	68.9	10.0	7.8	0.0	0.0	0.0	6.2	2.4	2.3
		240	55.8	66.5	10.8	7.0	0.0	1.1	0.0	6.9	3.0	2.4
		1440	100.0	63.3	10.5	7.6	0.0	1.3	1.5	7.3	3.3	3.2

POX: α-pinene oxide; CPA: campholenic aldehyde; ALD: iso-campholenic aldehyde; PCV: pinocarveol; PCP: pinocamphone; cis-CARV: cis-carveol; trans-CARV: trans-carveol; CRN: cis-caren-4-ol; HXN: 4-isopropenyl-1-methyl-2-cyclohexen-1-ol.

of them would have the same geometry and would favor the CPA production.

Taking into account that, when N_2 stream was used during calcinations, a higher magnetic blocking temperature and a lower specific surface area were obtained, it could be inferred that, clustering of the iron species occurs inside the MCM-41 channels. As a consequence, different crystalline planes, corners, steps, could be exposed and Fe^{3+} sites with appropriate geometry to be more active in adsorbing reactant would appear.

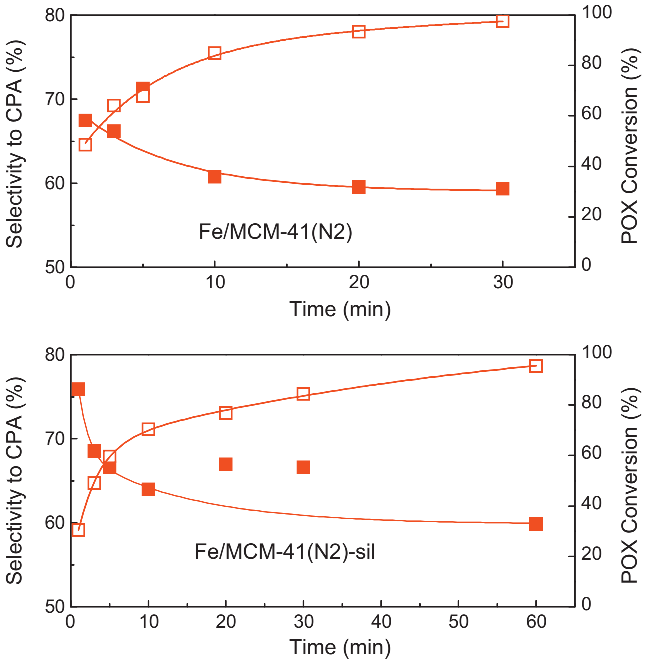

Fig. 9. Selectivity to α-campholenic aldehyde produced in the isomerization of α-pinene oxide (left axis, filled marker) and POX conversion (right axis, empty marker) vs. reaction time over Fe/MCM-41(N2) and Fe/MCM-41(N2)-sil catalysts.

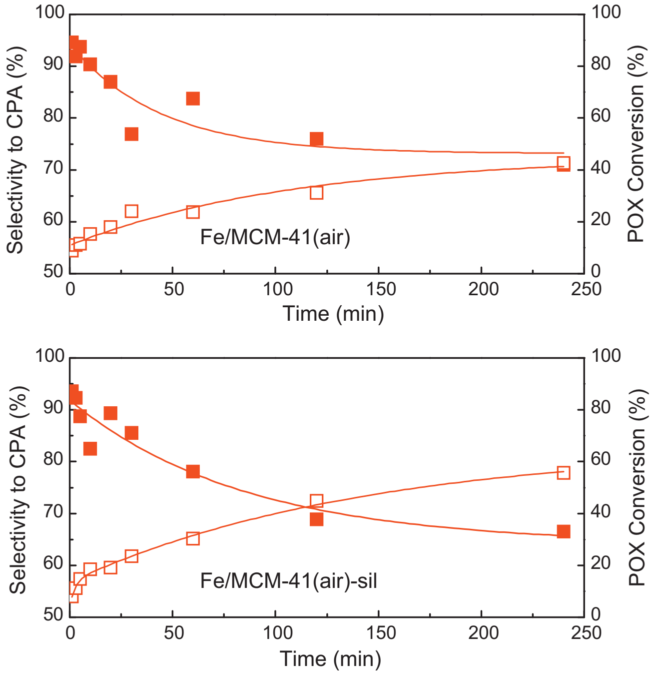

Fig. 10. Selectivity to α-campholenic aldehyde formed in the isomerization of α-pinene oxide (left axis, filled marker) and POX conversion (right axis, empty marker) vs. reaction time over Fe/MCM-41(air) and Fe/MCM-41(air)-sil catalysts.

4. Conclusions

Two Fe/MCM-41 systems calcined in different atmospheres (inert and oxidant) were studied. Both have extremely small α-Fe_2O_3 and/or amorphous Fe_2O_3 species. However, when air is used a more pronounced spreading with smaller size and a large oxide/support interaction was obtained.

In order to decrease the Brönsted acidity of the silanol groups present on the MCM-41, a silylation treatment over both series of catalysts was carried out. Their efficiency was verified by different techniques.

The POX isomerization allowed determining that the Brönsted acidity of the Fe/MCM-41 system has not the sufficient acid strength to decrease the selectivity towards CPA, since sylilated and non-sylilated samples have the same selectivity.

On the other hand, the different calcination atmospheres lead to different types of acid Lewis sites of Fe^{3+}. When air is used, the spreading conditions could be satisfied more easily, leading to the production of islands like as "raft" of iron oxide. Therefore, only one type of Fe^{3+} sites with high coordinative unsaturation is present. Instead, when the calcination was realized under N_2 stream, clustering of the iron species occurs inside the MCM-41 channels. As a consequence, more than one type of Fe^{3+} sites with appropriate geometry to POX isomerization appear. However, their geometry is less adequate in order to obtain a high CPA selectivity in comparison with the iron sites located on the iron "raft".

This study shows how it is be possible to tune the nature of the acid sites of a selected material by introducing new components; in this case highly unsaturated Fe species confirm to be good Lewis acid centers able to act as active sites in reactions requiring such sites.

Acknowledgement

The authors acknowledge the financial support of ANPCyT (PICT No. 00549), which allowed the development of this work.

References

[1] A. Corma, Chem. Rev. 97 (1997) 2373–2419.
[2] A. Corma, Chem. Rev. 95 (1995) 559–614.
[3] A. Corma, H. Garcia, Chem. Rev. 103 (2003) 4307–4365.
[4] G. Busca, Chem. Rev. 107 (2007) 5366–5410.
[5] G. Sartori, R. Maggi, Chem. Rev. 106 (2006) 1077–1104.
[6] Y. Sun, S. Walspurger, J.-P. Tessonier, B. Louis, J. Sommer, Appl. Catal. A 300 (2006) 1–7.
[7] N. He, S. Bao, Q. Xu, Appl. Catal. A 169 (1998) 29–36.
[8] A. Corma, V. Fornes, M.T. Navarro, J. Perez-Pariente, J. Catal. 148 (1994) 569–574.
[9] N. Ravasio, F. Zaccheria, A. Gervasini, C. Messi, Catal. Commun. 9 (2008) 1125–1127.
[10] R. Ryoo, J.M. Kim, J. Chem. Soc. Chem. Commun. (1995) 711–712.
[11] D.A.M. Monti, A. Baiker, J. Catal. 83 (1983) 323–335.
[12] K. Lagarec, D.G. Rancourt, Mossbauer spectral analysis software, Dep. of Phys. University of Otawa, Version 1.0., 1998.
[13] A. Gervasini, C. Messi, P. Carniti, A. Ponti, N. Ravasio, F. Zaccheria, J. Catal. 262 (2009) 224–234.
[14] R.R. Sever, R. Alcala, J. Dumesic, T.W. Root, Microporous Mesoporous Mater. 66 (2003) 53–67.
[15] J. Bu, H.K. Rhee, Catal. Lett. 66 (2000) 245–249.
[16] A. Gervasini, C. Messi, D. Flahaut, C. Guimon, Appl. Catal. A 367 (2009) 113–121.
[17] M. Ojeda, F.J. Pérez-Alonso, P. Terreros, S. Rojas, T. Herranz, M. López Granados, J.L. García Fierro, Langmuir 22 (2006) 3131–3137.
[18] R. Mariscal, M. Lòpez-Granados, J.L.G. Fierro, J.L. Sotelo, C. Martos, R. Van Grieken, Langmuir 16 (2000) 9460–9467.
[19] K. Lin, L. Wang, F. Meng, Z. Sun, Q. Yang, Y. Cui, D. Jiang, F.S. Xiao, J. Catal. 235 (2005) 423–427.
[20] S. Haukka, A. Root, J. Phys. Chem. 98 (1994) 1695–1703.
[21] E. Murad, J.H. Johnston, in: G.J. Long (Ed.), Mössbauer Spectroscopy Applied to Inorganic Chemistry, vol. 2, Plenum Publishing Corporation, 1987.
[22] S. Mørup, H. Topsøe, Appl. Phys. 11 (1976) 63–66.
[23] F. Bødker, S. Mørup, Europhys. Lett. 52 (2000) 217–223.
[24] M. Blume, J.A. Tjon, Phys. Rev. 165 (1968) 446–456.
[25] R.E. Vandenberghe, E. De Grave, C. Landuydt, L.H. Bowen, Hyperfine Interact. 53 (1990) 175–196.
[26] W.F. Brown Jr., Phys. Rev. 130 (1963) 1677–1686.
[27] A.M. Alvarez, J.F. Bengoa, M.V. Cagnoli, N.G. Gallegos, S.G. Marchetti, R.C. Mercader, Hyperfine Interact. 161 (2005) 3–9.
[28] S.H. Overbury, P.A. Bertrand, G.A. Somorjai, Chem. Rev. 75 (1975) 547–560.
[29] W.F. Holderich, J. Roseler, G. Heitmann, A.T. Liebens, Catal. Today 37 (1997) 353–366.
[30] L. Alaerts, E. Seguin, H. Poelman, F. Thibault-Starzyk, P.A. Jacobs, D.E. De Vos, Chem. Eur. J. 12 (2006) 7353–7363.
[31] J. Kaminska, M.A. Schwegler, A.J. Hoefnagel, H. van Bekkum, Recl. Trav. Chim. Pays-Bas 111 (1992) 432–437.
[32] G. Neri, G. Rizzo, S. Galvagno, G. Loiacono, A. Donato, M.G. Musolino, R. Pietropaolo, E. Rombi, Appl. Catal. A 274 (2004) 243–251.